ELSEVIER

Coordination Chemistry Reviews
211 (2001) 177–194

COORDINATION CHEMISTRY REVIEWS

www.elsevier.com/locate/ccr

The effects of electronic coupling and solvent broadening on the intervalent electron transfer of a centrosymmetric mixed-valence complex

David F. Watson, Andrew B. Bocarsly *

Department of Chemistry, Princeton University, Washington Road and William St., Princeton, NJ 08544, USA

Received 14 September 1999; accepted 10 January 2000

This contribution is dedicated to Professor Arthur Adamson on the occasion of his 80th birthday. Professor Adamson's contributions in the area of coordination photochemistry lay the groundwork for the studies reported here. His seminal work in the areas of photoinduced charge transfer processes and ligand substitution processes has paved the way for understanding the complex processes associated with multielectron charge transfer reactions and the photochemistry of supramolecular complexes. Much of today's mechanistic understanding of coordination chemistry is based on Professor Adamson's work. We are delighted that Professor Adamson has maintained his academic interest to this day and continues to play an important role in this field.

Contents

* Corresponding author. Tel.: +1-609-2583888; fax: +1-609-2582383.
E-mail address: bocarsly@chemvax.princeton.edu (A.B. Bocarsly).

0010-8545/01/$ - see front matter
PII: S0010-8545(00)00276-9

Abstract

A three-dimensional nuclear coordinate representation of the intervalent electron transfer processes occurring in the trinuclear mixed-valence complex, $[(NC)_5Fe(II)–CN–Pt(IV)(NH_3)_4–NC–Fe(II)(CN)_5]^{4-}$, is discussed in terms of the degree of coupling between electronic states. The related dinuclear complex, $(NC)_5Fe(II)–CN–Pt(IV)–(NH_3)_5$, has been synthesized and characterized by UV–vis and IR absorption spectroscopies, cyclic voltammetry, resonance Raman spectroscopy, and single crystal X-ray diffraction. The visible absorption spectra and time-dependent resonance Raman intensity analyses of the two complexes are compared with regard to the amount of electronic coupling in the trinuclear complex. The absorption spectrum of the trinuclear complex has been fit to a model, which includes a solvent broadening parameter. Based on this fit, the total reorganization energy of the photoinduced intervalent electron transfer has been calculated to be approximately 75% outer sphere.

Keywords: Electronic coupling; Solvent broadening; Mixed-valence complex; Resonance Raman

1. Introduction

Mixed-valence complexes are a class of inorganic compounds, which exhibit intervalent electron transfer (IT) between two metal centers. They have attracted a great deal of interest in recent years, due to their potential application in solar energy conversion, photocatalysis, and molecular electronics [1]. Our lab has previously reported the synthesis of the trimetallic, mixed-valence anion, $[(NC)_5Fe(II)–CN–Pt(IV)(NH_3)_4–NC–Fe(II)(CN)_5]^{4-}$ (herein referred to as Fe(II)–Pt(IV)–Fe(II)) from aqueous $K_3Fe(CN)_6$ and $Pt(NH_3)_4(NO_3)_2$ [2]. The absorption spectrum of Fe(II)–Pt(IV)–Fe(II) contains an intense band ($\varepsilon = 2365\ M^{-1}\ cm^{-1}$) centered at 424 nm. Irradiation into this band results in the dissociation of Fe(II)–Pt(IV)–Fe(II) into two equivalents of ferricyanide and one equivalent of platinum(II) tetrammine (collectively referred to as Fe(III)/Pt(II)/Fe(III)), which is a net two-electron transfer process [2]. The crystal structure of the platinum(II) tetrammine salt of Fe(II)–Pt(IV)–Fe(II) reveals that the complex possesses D_{4h} symmetry and is centrosymmetric about the platinum atom [2]. Since Fe(III)/Pt(II)/Fe(III) is also symmetric with respect to the inversion center of the complex, the simultaneous transfer of both electrons is symmetry-disallowed. Therefore, we have assigned the 424 nm band as the IT of one electron from Fe(II) to Pt(IV), yielding the reactive intermediate Fe(III)–Pt(III)–Fe(II). The intermediate then dissociates by a second, thermal IT from the remaining Fe(II) to Pt(III), yielding Fe(III)/Pt(II)/

Fe(III) [2]. A simplified description of these IT processes is given by the two-dimensional, three-parabola potential energy diagram shown in Fig. 1 [3,4].

2. Simplified time-dependent perturbation theory analysis of resonance Raman scattering intensity

An important parameter in understanding any photoinduced electron transfer process is the reorganization energy. According to classical Marcus–Hush theory, reorganization energy is defined according to Eq. (1), where λ is the reorganization energy, E_{op} is the energy of the absorption band maximum, and ΔG_{12} is the free energy

$$\lambda = E_{op} - \Delta G_{12} \quad (1)$$

difference between the ground vibrational states of the donor and acceptor electronic states [1e,f,5,6]. In other words, the reorganization energy is the degree of vibrational excitation of the acceptor, which occurs as a result of the absorption of light in a photoinduced electron transfer. The reorganization energy of the Fe(II) → Pt(IV) IT in Fe(II)–Pt(IV)–Fe(II) is labeled in Fig. 1. Reorganization energy can be partitioned into two components, the inner sphere and outer sphere reorganization energies. The inner sphere reorganization energy corresponds to the vibrational distortion of the donor–acceptor complex, while the outer sphere component corresponds to the distortion of the solvent [1e,5–11].

Tannor and Heller have developed a time-dependent perturbation theory analysis of resonance Raman scattering which enables the calculation of the inner sphere

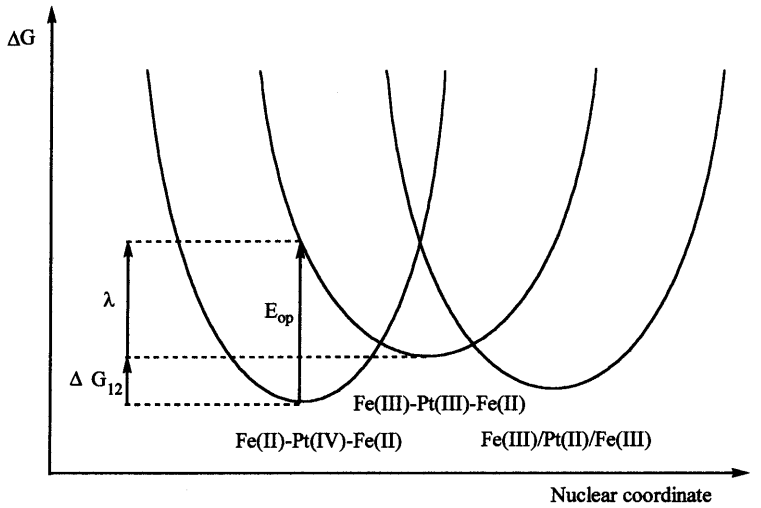

Fig. 1. Two-dimensional potential energy diagram of the electronic states involved in the photodissociation of Fe(II)–Pt(IV)–Fe(II).

reorganization energy of a photoinduced electron transfer, as well as the subdivision of the total inner sphere reorganization energy into components corresponding to each resonantly enhanced vibrational mode [12–15]. The intensity of Raman scattered light is proportional to the square of the derivative of the polarizability tensor with respect to the nuclear coordinate. A simplified expression for the polarizability tensor, derived by Tannor and Heller, is shown in Eq. (2), in which α_{fi} is the polarizability tensor, $\phi_i(\mathrm{t})$ is the time-evolving vibrational wavepacket

$$\alpha_{\mathrm{fi}} = \frac{2\pi i}{i}\langle \phi_{\mathrm{f}} | \phi_i(t) \rangle \exp[(i\Delta v - \Gamma)t]\, \mathrm{d}t \tag{2}$$

in the excited electronic state (the initial state in the Raman scattering process), ϕ_{f} is the first excited vibrational state of the ground electronic state (the final state in the Raman-scattering process), Δv is the difference between the frequency of incident light and the frequency of the electronic transition, and Γ is a damping factor [12,13]. In this equation, the polarizability tensor depends on the Franck–Condon overlap of ϕ_{f} and $\phi_i(t)$. If electronic states are modeled as harmonic oscillators, the overlap of ϕ_{f} and $\phi_i(t)$ depends on the force constants of the parabolas representing the ground and excited electronic states and the displacement of their minima along the nuclear coordinate axis [13,16]. The harmonic oscillator force constant relates to the bond strength, while the displacement of the ground and excited electronic states indicates the degree of nuclear distortion of the acceptor state which occurs as a result of the vertical electronic excitation [13,16]. Assuming that identical harmonic oscillator potentials describe the ground and excited electronic states, the relative intensities of resonance Raman bands are related to the nuclear coordinate displacements by Eq. (3), where I_d is the intensity, Δ_d is the unitless nuclear coordinate displacement, and v_d is the frequency of the dth

$$\frac{I_1}{I_2} = \frac{\Delta_1^2 v_1^2}{\Delta_2^2 v_2^2} \tag{3}$$

Raman band [12,13]. Absolute displacements are calculated from the absorption bandwidth of the electronic transition using Eq. (4), where $2\sigma^2$ is 25% of the square of the absorption bandwidth at 1/e of the maximum absorbance, and the

$$2\sigma^2 = \sum_d \Delta_d^2 v_d^2 \tag{4}$$

summation is over all resonantly enhanced Raman modes [12,13]. The inner sphere reorganization energy associated with each Raman mode (λ_d) can also be calculated based on Raman frequencies and intensities, using Eq. (5). The total inner sphere reorganization energy ($\lambda_{\mathrm{i.s.}}$) is the sum of the individual components associated

$$\lambda_d = \frac{1}{2}\Delta_d^2 v_d \tag{5}$$

Table 1
Summary of time-dependent resonance Raman analyses of Hupp's dinuclear, cyanide-bridged, mixed-valence complexes

Formula	Bandwidth (1/e) (cm^{-1})	Total $\lambda_{i.s.}$(cm^{-1})	% $\lambda_{i.s.}$ on IT axis	Reference
$(NC)_5Ru(II)–CN–Ru(III)(NH_3)_5^-$	5450	3980	44	[23]
$(NC)_5Fe(II)–CN–Os(III)(NH_3)_5^-$	4970	2850	38	[13]
$(NC)_5Fe(II)–CN–Ru(III)(NH_3)_5^-$	4930	2850	64	[24]

with each vibrational mode, as shown in Eq. (6) [12,13]. Several assumptions are implicit in the use of these intensity analysis equations [13]: (1) there is no mode-mixing (Duschinsky rotation) in the excited state [17], (2) only ground

$$\lambda_{i.s.} = \sum_d \lambda_d \tag{6}$$

vibrational states are occupied [18], (3) there is no Herzberg–Teller coupling of the first excited state to higher-lying excited states [19], (4) only a single electronic transition is resonantly enhanced [19,20], (5) the experimentally determined absorption bandwidth is due to a single absorption band [21], (6) the potential energy surfaces can be described as harmonic oscillators [12–15,21,22], and (7) scattering occurs under 'short-time' conditions [12,14,15].

The intensity analysis method of Tannor and Heller has been applied to several dinuclear, cyanide-bridged, mixed-valence complexes [13,19,20,23,24]. Table 1 summarizes the absorption bandwidths at 1/e of the maximum absorbance, the reported total inner sphere reorganization energies, and the contribution to the total inner sphere reorganization energies from vibrational modes directed along the IT axis for several of Hupp's complexes. In two of the three complexes, approximately 40% of the total inner sphere reorganization energy comes from vibrations along the IT axis [13,23,24].

3. Simplified time-dependent intensity analysis of resonance Raman scattering from Fe(II)–Pt(IV)–Fe(II) and implications on the nature of the photoinduced IT process

Our lab has previously reported an intensity analysis based on the resonance Raman spectra of Fe(II)–Pt(IV)–Fe(II) [21]. Table 2 shows the frequency, assignment, relative intensity, unitless nuclear coordinate displacement, and inner sphere reorganization energy associated with each resonantly enhanced Raman mode. Using Eq. (5), the total inner sphere reorganization energy was found to be 14 170 cm^{-1} with 457.9 nm incident light. Approximately 45% of the total inner sphere reorganization energy came from the ν(CN)-bridge, ν(Fe–C)-bridge, and ν(Pt–N)-bridge modes, which lie along the IT axis of the complex. This result corresponds well with Hupp's findings for the cyanide-bridged dinuclear complexes [13,23,24]

and is reasonable in light of the electron transfer axis. However, Fe(II)–Pt(IV)–Fe(II) deviated significantly from Hupp's dinuclear complexes in two regards: the 8400 cm^{-1} absorption bandwidth at 1/e of the maximum absorbance is considerably larger, and thus the total inner sphere reorganization energy is four to six times as large as those of the dinuclear complexes [13,21,23,24].

The Raman excitation profiles (REPs) of Fe(II)–Pt(IV)–Fe(II), shown in Fig. 2, are also somewhat unusual [21]. A REP is a plot of intensity versus incident frequency for a Raman band. For resonantly enhanced Raman bands, a REP should roughly resemble the absorption band of the corresponding electronic transition. In the case of Fe(II)–Pt(IV)–Fe(II), the REPs of the low-frequency (metal–ligand vibrational) modes are broad, but shifted to lower energy than the IT absorption band. The REPs of the high-frequency (cyanide stretching) modes are significantly narrower, and their maxima are near the IT absorption band maximum [21].

The surprisingly large absorption bandwidth and inner sphere reorganization energy, together with the unusual REPs, have raised some theoretical questions about the nature of the IT processes in Fe(II)–Pt(IV)–Fe(II). Due to the centrosymmetric nature of the complex, the transient intermediate which forms following irradiation into the IT band is doubly degenerate. That is, IT absorption equivalently leads to the formation of either Fe(III)–Pt(III)–Fe(II) or Fe(II)–Pt(III)–Fe(III). Therefore, there are two distinct nuclear coordinate axes involved in the photoinduced IT, so a three-dimensional potential energy surface is required to fully describe the IT processes in Fe(II)–Pt(IV)–Fe(II). The two-dimensional diagram in Fig. 1 is inadequate. In order to construct the required three-di-

Table 2
Resonance Raman data and time-dependent intensity analysis results for Fe(II)–Pt(IV)–Fe(II) in 0.5 M K_2SO_4 solution at 457.9 nm irradiation

ν (cm^{-1})	Assignment	Intensity[a]	Δ	λ_d (cm^{-1})	% of λ_{tot}
2123	ν(CN)-bridge	2.86	0.96	980	7
2103	ν(CN)-axial	0.42	0.37	150	1
2078	ν(CN)-radial	0.63	[b]	[b]	[b]
2062	ν(CN)-radial	0.98	[b]	[b]	[b]
623	ν(Fe–CN)-axial	2.44	3.03	2860	20
588	ν(Fe–CN)-radial	1.00	2.05	1240	9
566	ν(Fe–CN)-bridge	2.04	3.05	2630	19
505	ν(Pt–NH_3)	0.51	1.71	740	5
472	δ(Fe–CN)	0.70	2.14	1080	8
418	δ(Fe–CN)	0.20	1.29	350	2
364	ν(Pt–NC)-bridge	1.38	3.89	2760	19
295	δ(H_3N–Pt–NH_3)	1.56	3.06	1380	10

[a] The peak at 588 cm^{-1} has been arbitrarily assigned to an intensity of 1.00.

[b] The depolarization ratios of these modes indicate that they are non-totally symmetric [21], so the unitless nuclear coordinate displacement and inner sphere reorganization energy of these modes cannot be calculated using the intensity analysis method presented in the text.

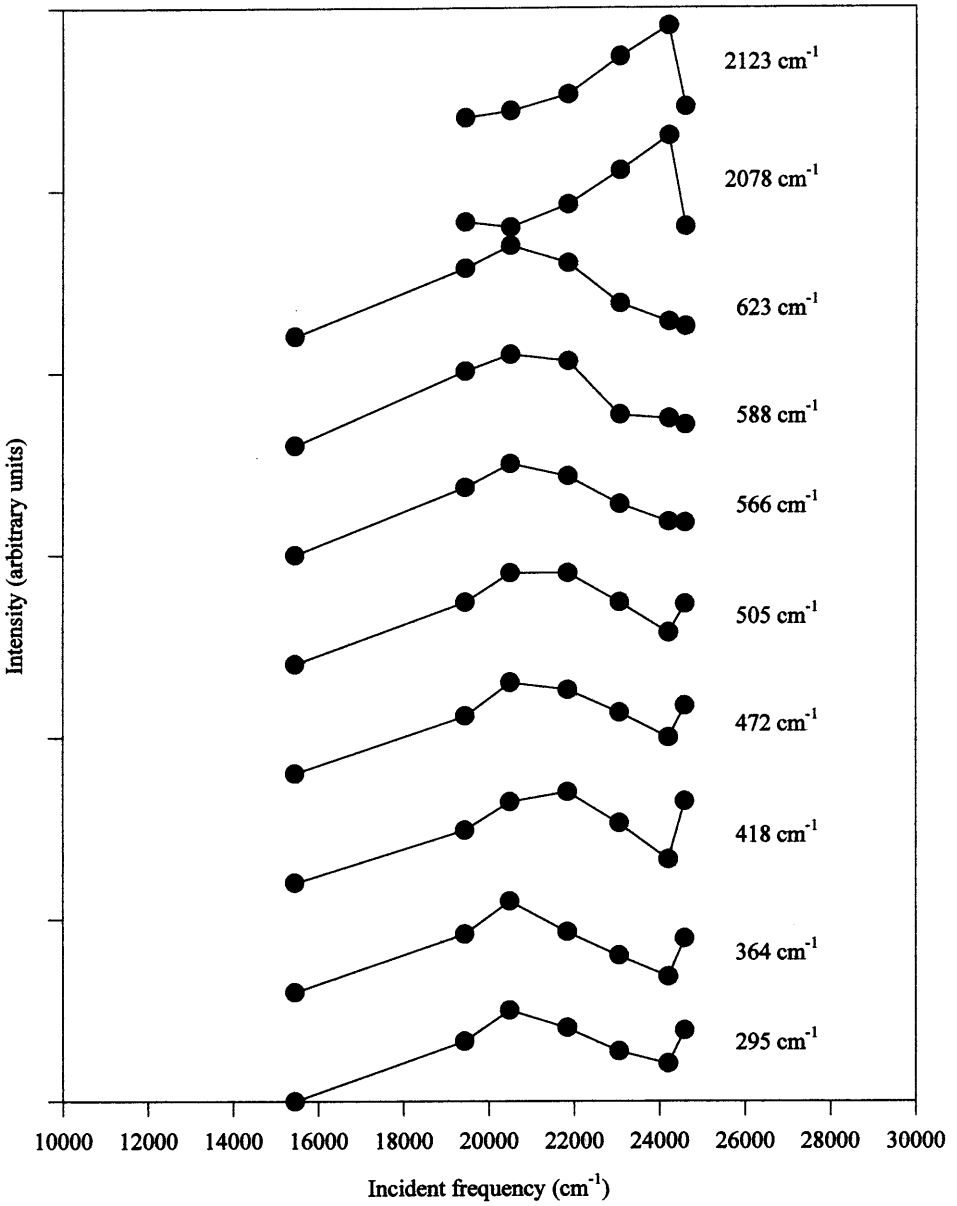

Fig. 2. Raman excitation profiles of Fe(II)–Pt(IV)–Fe(II) in 0.5 M K_2SO_4 at incident wavelengths of 406.7, 413.1, 443.8, 457.9, 488.0, 514.5, and 647.1 nm.

mensional diagram, we have assigned the Fe(III)–Pt(III)–Fe(II) intermediate to be caused by distortion along the '*x*' nuclear coordinate, while the Fe(II)–Pt(III)–Fe(III) intermediate is caused by distortion along the '*y*' nuclear

coordinate, as shown in Fig. 3(a) [22,25]. The three orthogonal axes of the potential energy diagram are shown in Fig. 3(b). If the photoinduced IT results in distortion along the x nuclear coordinate, then the second, thermal IT must cause distortion along the y coordinate, and vice-versa. The two symmetry-allowed pathways ($g \rightarrow u$, $u \rightarrow g$) are shown as solid lines in Fig. 3(c), and the symmetry-disallowed simultaneous transfer of both electrons ($g \rightarrow g$) is shown as a dotted line. The labeled points represent the minima of the potential energy surfaces (parabolic cones) corresponding to each electronic state involved in the IT process. The transformation of the nuclear coordinate system from the x and y coordinate axes into the symmetric ($[x+y]/\sqrt{2}$) and antisymmetric ($[x-y]/\sqrt{2}$) linear combinations is shown in Fig. 3(d). The projection of the three-dimensional potential energy surfaces of the four electronic states onto the plane defined by the energy axis and the symmetric nuclear coordinate is shown in Fig. 3(e). This projection is equivalent to the original two-dimensional potential energy diagram of Fig. 1. The projection of the potential energy surfaces of the electronic states onto the plane defined by the energy axis and the antisymmetric nuclear coordinate is shown in Fig. 3(f). The antisymmetric projection illustrates that the Fe(II)–Pt(III)–Fe(III) and Fe(III)–Pt(III)–Fe(II) potential energy surfaces may overlap [22,25]. If a significant degree of electronic coupling between these two surfaces occurs, two nondegenerate states would result, giving rise to two different IT energies and a broader IT absorption band. This situation is shown in Fig. 3(g), in which 2 J is the degree of electronic coupling between the two electronic states. A similar coupling of electronic states has been proposed by Scandola and co-workers for a Ru(II)–Ru(III)–Ru(II) complex capable of undergoing photoinduced $Ru(II) \rightarrow Ru(III)$ IT from either of the two Ru(II) atoms [26].

The splitting of the two reactive intermediate electronic states into nondegenerate states might explain the exceptionally broad absorption bandwidth of the Fe(II)–Pt(IV)–Fe(II) IT band and the large inner sphere reorganization energy calculated with the time-dependent Raman intensity analysis. Furthermore, the differences between the metal–ligand and cyanide band REPs could be accounted for by the presence of two IT absorptions. If two transitions existed, then the

Fig. 3. Symmetry-based analysis of the photoinduced IT process in Fe(II)–Pt(IV)–Fe(II). (a) Photoinduced IT causes distortion along the 'x' nuclear coordinate to form Fe(III)–Pt(III)–Fe(II) or along the 'y' nuclear coordinate to form Fe(II)–Pt(III)–Fe(III). (b) The three orthogonal axes of the potential energy versus nuclear coordinate diagram. (c) The plane defined by the x and y nuclear coordinate axes, in which the labeled points correspond to the minima of the potential energy surfaces (parabolic cones) representing each electronic state. The symmetry-allowed sequential IT pathways are shown by solid lines, while the symmetry-forbidden simultaneous transfer of two electrons is shown by the dashed line. (d) Linear combinations of the x and y nuclear coordinates yield the symmetric, ($[x+y]/\sqrt{2}$), and antisymmetric, ($[x-y]/\sqrt{2}$), nuclear coordinate axes. (e) Projection of the four potential energy surfaces onto the plane defined by the energy axis and the symmetric nuclear coordinate. (f) Projection of the potential energy surfaces onto the plane defined by the energy axis and the antisymmetric nuclear coordinate. The potential energy surface of Fe(III)/Pt(II)/Fe(III) has been omitted for clarity. (g) Qualitative representation of the possible electronic coupling between the degenerate Fe(III)–Pt(III)–Fe(II) and Fe(II)–Pt(III)–Fe(III) states. Coupling would produce two nondegenerate IT transitions with energies E_{op1} and E_{op2}.

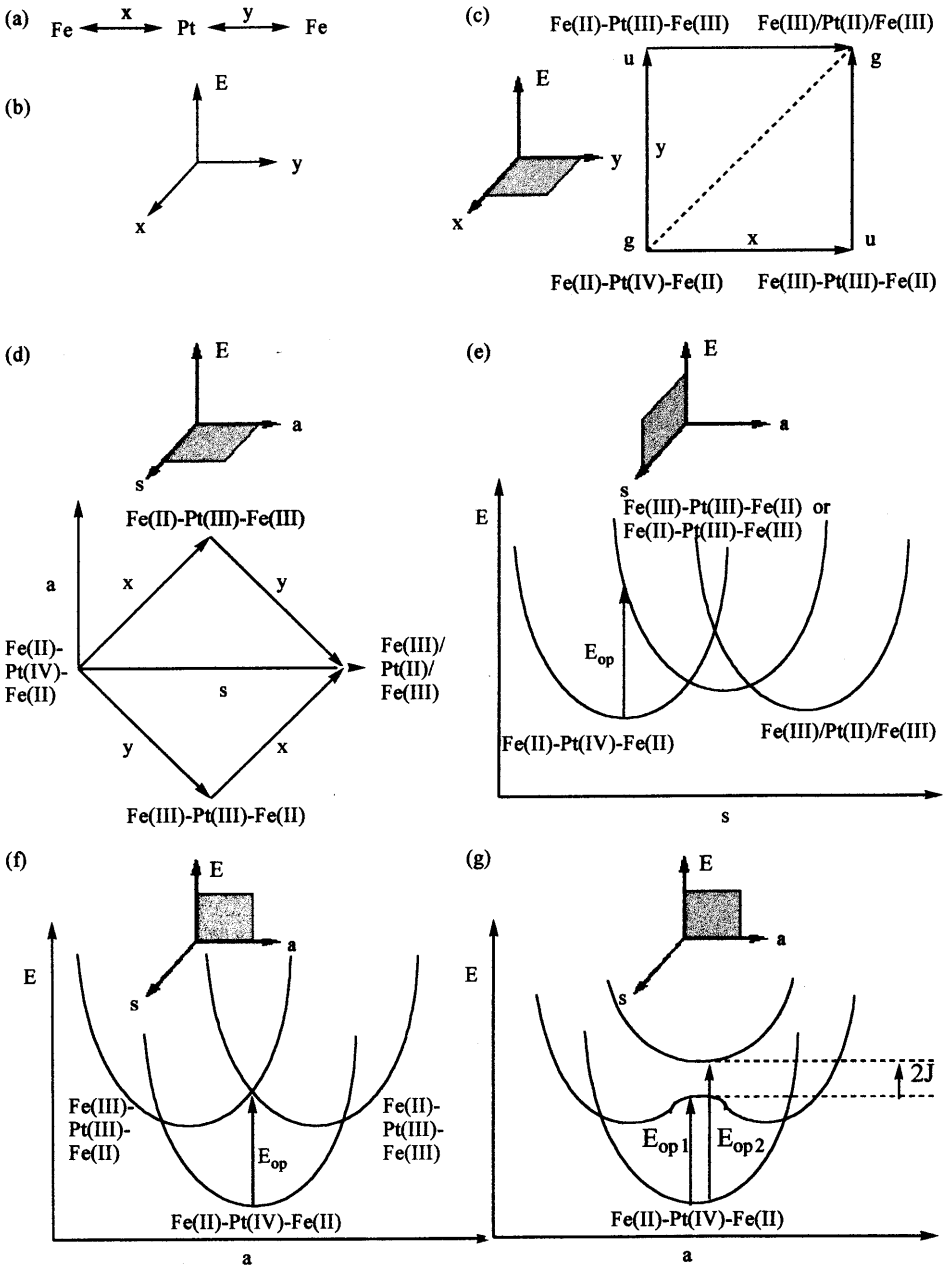
(a)
Fe
x
Pt
y
Fe
(b)
E
y
x
(c)
Fe(II)-Pt(III)-Fe(III)
Fe(III)/Pt(II)/Fe(III)
E
u
g
y
y
x
g
x
u
Fe(II)-Pt(IV)-Fe(II)
Fe(III)-Pt(III)-Fe(II)
(d)
E
a
s
Fe(II)-Pt(III)-Fe(III)
a
x
y
Fe(II)-
Pt(IV)-
Fe(II)
s
Fe(III)/
Pt(II)/
Fe(III)
y
x
Fe(III)-Pt(III)-Fe(II)
(e)
E
a
s
Fe(III)-Pt(III)-Fe(II) or
Fe(II)-Pt(III)-Fe(III)
E
E_op
Fe(II)-Pt(IV)-Fe(II)
Fe(III)/Pt(II)/Fe(III)
s
(f)
E
a
s
E
Fe(III)-
Pt(III)-
Fe(II)
E_op
Fe(II)-
Pt(III)-
Fe(III)
Fe(II)-Pt(IV)-Fe(II)
a
(g)
E
a
s
E
2J
E_op1
E_op2
Fe(II)-Pt(IV)-Fe(II)
a

Fig. 3.

Raman modes associated with the transition closest in energy to that of the incident light would be selectively enhanced. The maxima of the REPs of modes associated with the higher-energy IT transition would be shifted to higher frequency than the maxima of the REPs of modes associated with the lower-energy transition.

On the other hand, if the potential energy surfaces of Fe(II)–Pt(III)–Fe(III) and Fe(III)–Pt(III)–Fe(II) do not overlap significantly, or if little or no electronic coupling occurs as a result of their overlap, then the two reactive intermediates would remain degenerate, and only one IT energy would exist. In this case, Fe(II)–Pt(IV)–Fe(II) would best be described as a pair of noninteracting back-to-back donor–acceptor complexes which happen to share the same acceptor atom (Fe(II)–Pt(IV), Pt(IV)–Fe(II)).

4. Synthesis and characterization of $(NC)_5Fe(II)$–CN–Pt(IV)–$(NH_3)_5$ as a model for Fe(II)–Pt(IV)–Fe(II)

In order to investigate the possibility of coupled excited states in Fe(II)–Pt(IV)–Fe(II), the dinuclear species $(NC)_5Fe(II)$–CN–Pt(IV)–$(NH_3)_5$ (herein referred to as Fe(II)–Pt(IV)) has recently been synthesized [25]. This complex was chosen because it should be capable of the same primary photoinduced Fe(II)→Pt(IV) IT as in the trinuclear complex. Since there is only one iron atom in the dinuclear complex, there is no possibility of coupled reactive intermediate electronic states giving rise to two IT energies. Therefore, the absorption bandwidth and inner sphere reorganization energy of the dinuclear complex should provide insight into whether or not significant electronic coupling occurs in the trinuclear complex.

Fe(II)–Pt(IV) was synthesized by the reaction of aqueous solutions of $[Pt(NH_3)_5(OSO_2CF_3)](OSO_2CF_3)_3$ and $K_4Fe(CN)_6$ in equimolar amounts. When the solutions were combined, the mixture developed a red–orange color with a broad electronic absorption band centered at 421 nm. This band was assigned as the Fe(II)→Pt(IV) IT absorption, by analogy with the band centered at 424 nm in the Fe(II)–Pt(IV)–Fe(II) spectrum [2,25]. The IT bandwidth at 1/e of the maximum absorbance for Fe(II)–Pt(IV) was 8400 cm^{-1}, identical to that of the trinuclear complex. The IR spectrum of Fe(II)–Pt(IV) contained two cyanide stretching bands (2119 and 2054 cm^{-1}), indicating the presence of bridging and terminal cyanide ligands, respectively [25]. These cyanide stretch frequencies correspond very closely with those which were observed for Fe(II)–Pt(IV)–Fe(II) [2]. The IR spectrum contained a band at 585 cm^{-1}, which is indicative of an Fe–C stretch for iron in the +2 oxidation state [25,27]. Bands were also observed at 3000–3200, 1399, and 989 cm^{-1}, corresponding to typical frequencies of N–H stretching modes, symmetric H–N–H bending modes, and NH_3 rocking modes in Pt(IV) ammine complexes [25]. The IR spectrum provides evidence that the dinuclear complex was formed and that both metals remain in their initial oxidation states in the complex. Cyclic voltammetry was performed on Fe(II)–Pt(IV) in 1 M $NaNO_3$ solution, revealing a

single, quasi-reversible wave with $E_{1/2} = 0.53$ V vs. SCE [25]. This peak was assigned as the Fe(II)/(III) couple, based on a similar $E_{1/2} = 0.55$ V vs. SCE for Fe(II)–Pt(IV)–Fe(II) [2,25].

The crystal structure of Fe(II)–Pt(IV) provided further evidence for the occurrence of the Fe(II) → Pt(IV) IT. The Fe and Pt radial ligands are in a *gauche* conformation, such that the Fe $3d_{xy}$ orbital is aligned parallel to the Pt $5d_{x^2-y^2}$ orbital [25]. This arrangement allows for the spatial overlap of these orbitals, which are the donating and accepting orbitals in the IT process. This same *gauche* conformation was observed in the crystal structure of Fe(II)–Pt(IV)–Fe(II) and provides the required electronic coupling for electron transfer between the two orbitals [2].

5. Resonance Raman spectroscopy of Fe(II)–Pt(IV) and simplified time-dependent intensity analysis

Resonance Raman spectra of 40 mM aqueous solutions of Fe(II)–Pt(IV), with 0.5 M K_2SO_4 as an internal intensity standard, were obtained at incident wavelengths of 406.7, 413.1, 457.9, and 472.7 nm, using either a krypton ion or argon ion laser. Spectra of the low frequency, metal–ligand vibrational modes were also obtained at higher excitation wavelengths. The observed spectra were baseline-corrected, multiplied by the square of the wavelength of Raman scattered light to correct for the wavelength dependence of the detector entrance slit, and normalized using the intensities of the internal sulfate standard. The Raman spectrum obtained

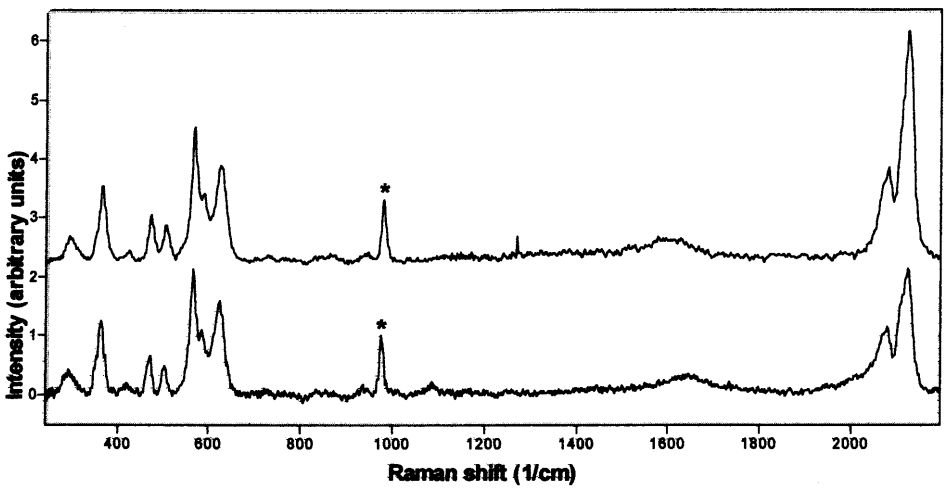

Fig. 4. Resonance Raman spectra of Fe(II)–Pt(IV) at 472.7 nm irradiation (top spectrum) and Fe(II)–Pt(IV)–Fe(II) at 476.5 nm irradiation (bottom spectrum) in 0.5 M K_2SO_4. The sulfate band is marked with an asterisk in each spectrum. Frequencies and assignments of Raman bands are shown in Tables 2 and 3.

Table 3
Resonance Raman data and time-dependent intensity analysis results for Fe(II)–Pt(IV) in 0.5 M K_2SO_4 solution at 457.9 nm irradiation

ν (cm^{-1})	Assignment	Intensity[a]	Δ	λ_d (cm^{-1})	% of λ_{tot}
2125	ν(CN)-bridge	4.39	1.14	1390	11
2107	ν(CN)-axial	0.51	0.39	160	1
2082	ν(CN)-radial	0.88	[b]	[b]	[b]
2069	ν(CN)-radial	0.84	[b]	[b]	[b]
628	ν(Fe–C)-axial	2.11	2.68	2250	18
590	ν(Fe–C)-radial	1.00	1.96	1130	9
570	ν(Fe–C)-bridge	1.70	2.65	2010	16
508	ν(Pt–NH_3)	0.42	1.48	560	4
475	δ(Fe–CN)	0.69	2.01	970	8
426	δ(Fe–CN)	0.25	1.36	390	3
368	ν(Pt–NC)	1.54	3.90	2800	22
298	δ(H_3N–Pt–NH_3)	0.53	2.78	1170	9

[a] The peak at 590 cm^{-1} has been arbitrarily assigned to an intensity of 1.00.
[b] The depolarization ratios of the corresponding modes in Fe(II)–Pt(IV)–Fe(II) indicate that they are non-totally symmetric [21], so the unitless nuclear coordinate displacement and inner sphere reorganization energy of these modes cannot be calculated using the intensity analysis method presented in the text.

with 472.7 nm incident light is shown in Fig. 4, along with that of Fe(II)–Pt(IV)–Fe(II) at 476.5 nm. An intensity analysis of the Raman data was performed using Eqs. (3)–(6). Table 3 lists the frequency, assignment, relative intensity, unitless normal coordinate displacement, and inner sphere reorganization energy of each Raman mode for Fe(II)–Pt(IV) with 457.9 nm excitation. The REPs of the six most intense Raman modes of Fe(II)–Pt(IV) are shown in Fig. 5.

There is striking similarity between the Raman spectra of Fe(II)–Pt(IV) and Fe(II)–Pt(IV)–Fe(II) [21,25]. The same number of modes was resonantly enhanced in each of the two complexes, and their frequencies and relative intensities were virtually identical. Since the two complexes have the same IT bandwidth, the Raman intensity analysis results were nearly identical as well. The total inner sphere reorganization energy of Fe(II)–Pt(IV) was calculated to be 12 830 cm^{-1} based on the 457.9 nm Raman spectrum. The total inner sphere reorganization energy of the trinuclear complex was found to be 14 170 cm^{-1} at the same incident wavelength. The unitless nuclear coordinate displacements and individual inner sphere reorganization energies of each Raman band were nearly identical in the two complexes. For both complexes, approximately 45% of the total inner sphere reorganization energy corresponded to vibrations along the Fe–Pt axis. The REPs of Fe(II)–Pt(IV) were also very similar to those of the trinuclear complex. The metal–ligand REPs were broad and slightly red-shifted from the IT absorption maximum, while the cyanide REPs were significantly sharper with maxima near that of the IT band.

If coupling of the reactive intermediate electronic states were occurring in Fe(II)–Pt(IV)–Fe(II), its IT absorption bandwidth would be greater than that of Fe(II)–Pt(IV), due to the presence of two nondegenerate IT absorptions. In

addition, a greater number of Raman modes would be resonantly enhanced in the trinuclear complex than in the dinuclear complex, and the REPs would look

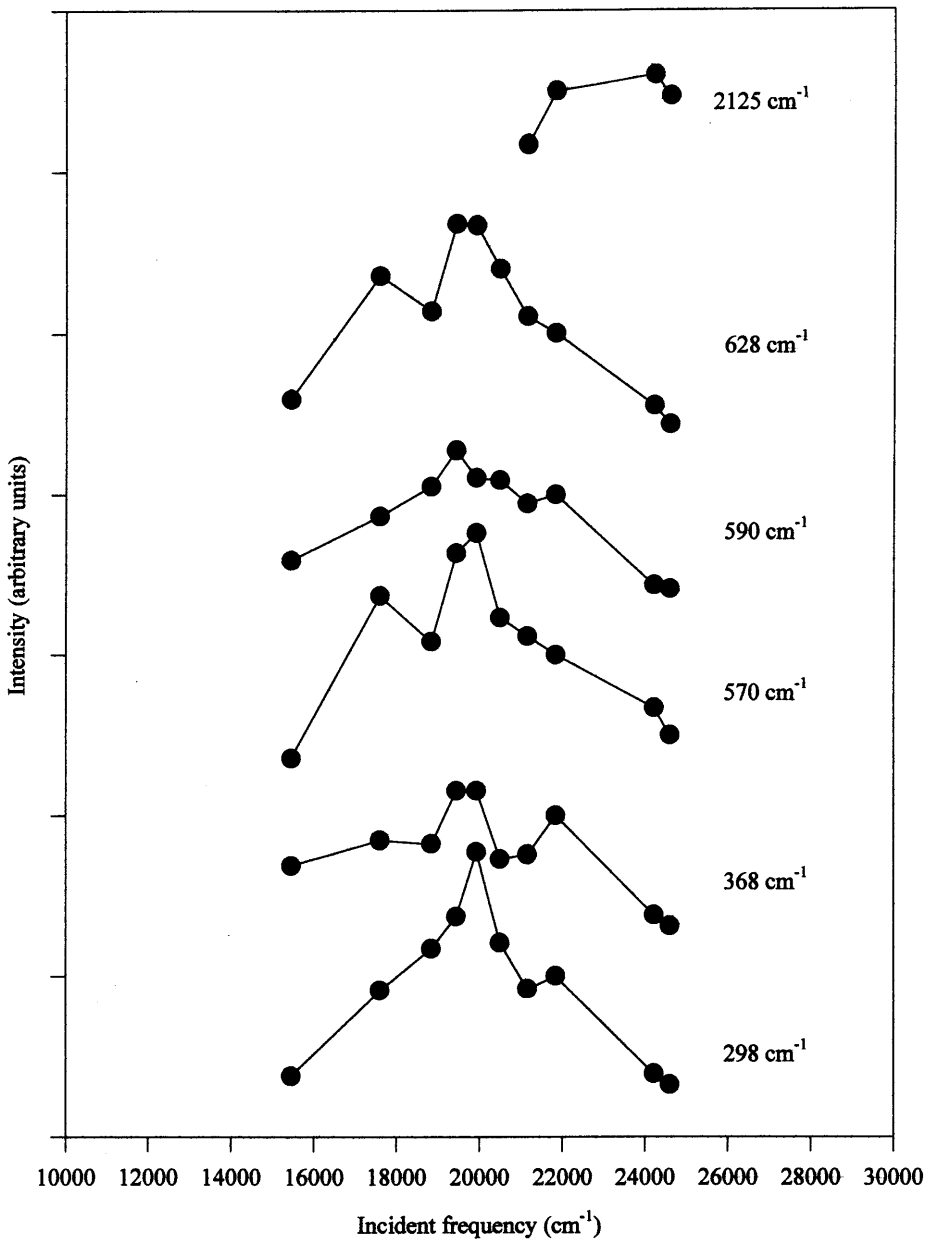

Fig. 5. Raman excitation profiles of the six most intense bands of Fe(II)–Pt(IV) in 0.5 M K_2SO_4 solution at incident wavelengths of 406.7, 413.1, 457.9, 472.7, 488.0, 501.7, 514.5, 530.9, 568.2, and 647.1 nm.

different. None of these characteristics were observed. In light of the similarity between the IT absorption bands, Raman spectra, and Raman intensity analyses of the two complexes, it must be concluded that the coupling of transient intermediate electronic states does not contribute significantly to the large IT bandwidth, large reorganization energy, or unusual REPs of Fe(II)–Pt(IV)–Fe(II). Instead, Fe(II)–Pt(IV)–Fe(II) can be accurately approximated as a pair of donor–acceptor complexes with localized oxidation states which happen to share the same acceptor.

6. Alternative explanations for the large absorption bandwidth and unusual REPs of Fe(II)–Pt(IV)–Fe(II) and Fe(II)–Pt(IV)

Both of the complexes under investigation yield ferricyanide as a dissociation product following excitation into the IT band. The visible absorption spectrum of ferricyanide contains an LMCT band centered at 420 nm, which is significantly narrower than the IT bands of Fe(II)–Pt(IV)–Fe(II) and Fe(II)–Pt(IV). If the Raman samples were dissociating significantly in the laser beam, then resonance enhancement of the ferricyanide modes associated with the LMCT process could be observed at low incident wavelengths. This would explain the observed sharpness of the cyanide band REPs and the shift of their maxima to higher frequency than the maxima of the metal–ligand REPs. The high frequency region of the aqueous ferricyanide Raman spectrum contains a single, broad cyanide band centered at 2135 cm^{-1} [28], which is slightly higher in frequency than the μ-CN band of Fe(II)–Pt(IV)–Fe(II). If the ferricyanide band were resonantly enhanced, the observed band centered at 2125 cm^{-1} would broaden and shift to higher frequency, due to the overlap of the ferricyanide and Fe(II)–Pt(IV)–Fe(II) bands. No change in the μ-CN bandshape or frequency maximum was observed in the low incident wavelength spectra. In addition, both the terminal-CN and μ-CN bands of Fe(II)–Pt(IV)–Fe(II) were selectively enhanced at high incident frequencies. Since the ferricyanide Raman spectrum only contains a single cyanide band, both bands would not be enhanced as a result of the ferricyanide LMCT absorption. Therefore, it was concluded that the Fe(II)–Pt(IV)–Fe(II) sample does not dissociate significantly enough in the laser beam to give rise to observable resonantly enhanced ferricyanide bands.

The large absorption bandwidth and the unusual shapes of the cyanide band REPs could also be explained by the overlap of an MLCT band with the high-frequency end of the IT absorption band. In ferrocyanide, the Fe $3d \rightarrow CN$ π^* MLCT band is centered at 295 nm. The Fe(II)/(III) redox potentials in Fe(II)–Pt(IV)–Fe(II) and Fe(II)–Pt(IV) are approximately 300 mV more positive than in ferrocyanide, due to the withdrawal of electron density from the iron centers upon binding to platinum [2]. The lowering of the Fe 3d energies should cause a blue shift in the MLCT absorption bands of Fe(II)–Pt(IV)–Fe(II) and Fe(II)–Pt(IV) relative to that of ferrocyanide. Therefore, the overlap of an MLCT band with the IT absorption is probably insignificant.

Solvent broadening is a more likely cause of the large absorption bandwidths of Fe(II)–Pt(IV)–Fe(II) and Fe(II)–Pt(IV). Solvent broadening can occur in mixed-valence complexes due to their polar nature. Immediately following the IT process, the solvent surrounding the newly oxidized metal is polarized as it was for the metal in its reduced form, and vice-versa for the solvent surrounding the newly reduced metal [5b,6b–d,29,30]. The rearrangement of solvent molecules contributes to solvent reorganization energy, which in turn contributes to the energy of the IT transition [5b,6b–d,29,30]. A distribution of solvation interactions leads to a distribution of IT energies and results in the overall broadening of the IT absorption band. Fe(II)–Pt(IV)–Fe(II) and Fe(II)–Pt(IV) should be particularly susceptible to solvent-broadening, due to large dipolar interactions and strong hydrogen bonding involving the terminal cyanide ligands. Irradiation into the IT band, and the subsequent change in the oxidation state of the metal ions, should cause a significant change in the optimal solvation of the complexes, which in turn should cause a large solvent reorganization energy term and a broadening of the absorption band.

The absorption spectrum of a related complex, $[(NC)_5$–Fe(II)–CN–Pt(IV)$(en)_2$–NC–Fe(II)–$(CN)_5]^{4-}$, where 'en' is ethylenediammine, has been obtained in various solvents [4]. The IT energy was found to vary extensively with solvent. Gutmann's acceptor number scale [31] was used to investigate the relationship between IT energy and solvent electron-accepting ability. A linear relationship between IT energy and solvent acceptor number was observed, suggesting that the degree of hydrogen bonding between terminal cyanide ligands and solvent molecules plays an important role in the IT energetics [4]. In addition, the absorption spectrum of Fe(II)–Pt(IV)–Fe(II) has been obtained in acetonitrile/water, DMSO/water, and formamide/water mixed solvents. In all three mixtures, the absorption maximum shifted to lower energy, and the bandwidth increased. The variation of the IT absorption maximum and bandwidth with solvent provides evidence that a significant portion of the bandwidth may be due to solvent broadening.

7. Calculation of outer sphere reorganization energy using revised time-dependent analysis of absorption and resonance Raman spectra

In mixed-valence complexes which exhibit strong solvent broadening, vibrational modes of the complex are coupled to solvent vibrational modes. Therefore, it is probably an oversimplification to assume that the reorganization energy calculated using Tannor and Heller's method is strictly inner sphere. Barbara and co-workers have estimated that the reorganization energies reported for two of Hupp's dinuclear complexes are approximately 65% outer sphere, based on the inclusion of solvent broadening in the calculated absorption spectra of the complexes [32,33]. Hennessy and Soos have also recently derived an expression for the calculation of electronic absorption spectra, which involves a solvent broadening parameter. This expression is shown in Eq. (7) [22], in which I is the intensity of absorbed light, x

is the frequency, σ_s is the solvent broadening parameter, t is time, Γ is a damping factor, ϕ_o is the ground vibrational state of the ground

$$I(x, \sigma_s) = -\mathrm{Re}\int_0^\infty \mathrm{d}t\ \exp[t(ix - \Gamma - \frac{1}{2}\sigma_s^2 t)]\langle\phi_o|\ \exp(it\sum_j \omega_j b_j^+ b_j)\ |\ \phi_i(t)\rangle/\pi \tag{7}$$

electronic state, $\phi_i(t)$ is a time-evolving vibrationally excited state in the electronic excited state, ω_j is the frequency of the j^{th} vibrational mode, and b_j^+ and b_j are boson operators which create and annihilate a quantum $(h\omega_j)/2\pi$ [22]. Note that the intensity of absorption depends on the overlap of ϕ_o and $\phi_i(t)$. This is analogous to Raman scattering intensity, but with different initial and final states. The overlap integral can be reduced to the expression shown in Eq. (8), in which g_j is a unitless normal coordinate displacement ($g_j = \Delta_j/\sqrt{2}$, where Δ_j is the normal coordinate displacement presented in the prior Heller analysis).

$$\langle\phi_o|\phi_i(t)\rangle = \exp\left(\sum_j g_j^2(e^{i\omega_j t} - 1)\right) \tag{8}$$

In order to fit the absorption spectrum of the centrosymmetric Fe(II)–Pt(IV)–Fe(II) complex, Hennessy and Soos derived integrals for the overlap of a vibrational wavefunction in the ground electronic state with a time-evolving vibrational wavefunction in either the symmetric or antisymmetric linear combination of the Fe(III)–Pt(III)–Fe(II) and Fe(II)–Pt(III)–Fe(III) electronic states [22]. The expressions are shown in Eqs. (9) and (10) for the symmetric and antisymmetric linear combinations, respectively.

$$\langle\phi_o|\phi_i(t)\rangle = \left(\exp\left[-\vec{g}\cdot\vec{g} + \sum_s g_s^2 e^{i\omega_s t}\right]\right)\sinh\left(\sum_a g_a^2 e^{i\omega_a t}\right) \tag{9}$$

$$\langle\phi_o|\phi_i(t)\rangle = \left(\exp\left[-\vec{g}\cdot\vec{g} + \sum_s g_s^2 e^{i\omega_s t}\right]\right)\cosh\left(\sum_a g_a^2 e^{i\omega_a t}\right) \tag{10}$$

The experimentally observed IT absorption band was fit to Eq. (7), using the overlap integrals in Eqs. (9) and (10), and varying the values of J, λ_i, σ_s, and Γ. The best fit occurred with $J = -1800\ \mathrm{cm}^{-1}$, $\lambda_i = 1800\ \mathrm{cm}^{-1}$, $\sigma_s = 1500\ \mathrm{cm}^{-1}$, and $\Gamma = 5\ \mathrm{cm}^{-1}$ [22]. The calculated inner-sphere reorganization energy of 1800 cm^{-1} is almost an order of magnitude less than the original estimation of 14 170 cm^{-1} [22]. The outer sphere reorganization energy was calculated to be 6000 cm^{-1}, or 75% of the total reorganization energy, based on Eq. (11) and a temperature of 300 K [34]. The value of J used in the fitting was probably an

$$\sigma_s^2 = 2\lambda_{\text{o.s.}} kT \tag{11}$$

overestimation, based on the fact that the Fe(II)–Pt(IV) absorption and Raman spectra have since suggested a negligible degree of electronic coupling in the trinuclear complex. However, when the IT absorption band of Fe(II)–Pt(IV)–Fe(II) was fit with $J = 0$ (no coupling between the electronic states of the two intermediates), the resulting nuclear coordinate displacements and inner sphere reorganiza-

tion energy were still significantly lower than the original estimations, and the majority of the total reorganization energy was outer sphere [22].

8. Conclusions

The absorption and Raman spectra of Fe(II)–Pt(IV) have shown that Fe(II)–Pt(IV)–Fe(II) can be accurately modeled as a valence-localized pair of donor–acceptor complexes with minimal electronic coupling between degenerate intermediate states. Solvent reorganization comprises the majority of the total reorganization energy of the photoinduced IT in Fe(II)–Pt(IV)–Fe(II), and must be accounted for in time-dependent resonance Raman intensity analysis calculations.

Acknowledgements

We thank Z. Soos and M. Hennessy for their theoretical analysis, and T. Spiro for the use of his Raman instrumentation. This work was supported by the National Science Foundation under grant number CHE-9631380.

References

[1] (a) B.S. Brunschwig, C. Creutz, N. Sutin, Coord. Chem. Rev. 177 (1998) 61. (b) T.J. Meyer, Chem. Rev. 98 (1998) 1439. (c) F. Scandola, M.T. Indelli, C. Chiorboli, C.A. Bignozzi, Top. Curr. Chem. 158 (1990) 73. (d) A. Vogler, A.H. Osman, H. Kunkely, Coord. Chem. Rev. 64 (1985) 159. (e) T.J. Meyer, Acc. Chem. Res. 11 (1978) 94. (f) C. Creutz, Prog. Inorg. Chem. 30 (1983) 1.
[2] M. Zhou, B.W. Pfennig, J. Steiger, D. Van Engen, A.B. Bocarsly, Inorg. Chem. 29 (1990) 2456.
[3] B.W. Pfennig, A.B. Bocarsly, J. Phys. Chem. 96 (1992) 226.
[4] Y. Wu, C. Cohran, A.B. Bocarsly, Inorg. Chim. Acta 226 (1994) 251.
[5] (a) R.A. Marcus, J. Chem. Phys. 24 (1956) 966. (b) R.A. Marcus, J. Chem. Phys. 43 (1965) 679. (c) R.A. Marcus, N. Sutin, Inorg. Chem. 14 (1975) 213.
[6] (a) N.S. Hush, Trans. Faraday Soc. 57 (1961) 557. (b) N.S. Hush, Prog. Inorg. Chem. 8 (1967) 391. (c) N.S. Hush, Electrochim. Acta 13 (1968) 1005. (d) N.S. Hush, Chem. Phys. 10 (1975) 361.
[7] N. Sutin, in: G.L. Eichborn (Ed.), Inorganic Biochemistry, vol. 2, Elsevier, New York, 1973.
[8] N.R. Kestner, J. Logan, J. Jortner, J. Phys. Chem. 78 (1974) 2148.
[9] P.P. Schmidt, J. Chem. Phys. 56 (1972) 2775.
[10] V.G. Levich, Adv. Electrochem. Eng. 4 (1966) 249.
[11] R.R. Degonadze, in: N.S. Hush (Ed.), Reactions of Molecules at Electrodes, Oxford University Press, London, 1971.
[12] D. Tannor, E.J. Heller, J. Chem. Phys. 77 (1982) 202.
[13] S.K. Doorn, R.L. Blackbourne, C.S. Johnson, J.T. Hupp, Electrochim. Acta 36 (1991) 1775.
[14] E.J. Heller, Acc. Chem. Res. 14 (1981) 368.
[15] E.J. Heller, R.L. Sundberg, D. Tannor, J. Phys. Chem. 86 (1982) 1822.
[16] A.B. Meyers, R.A. Mathies, in: T.G. Spiro (Ed.), Biological Applications of Raman Spectroscopy, Wiley, New York, 1988.
[17] D.E. Morris, W.H. Woodruff, J. Phys. Chem. 89 (1985) 5795.
[18] K.T. Schomacker, P.M. Champion, J. Chem. Phys. 90 (1989) 5982.
[19] K.S. Shin, J.I. Zink, J. Am. Chem. Soc. 112 (1990) 7148.

[20] J.L. Wootton, J.I. Zink, J. Am. Chem. Soc. 119 (1997) 1895.
[21] B.W. Pfennig, Y. Wu, R. Kumble, T.G. Spiro, A.B. Bocarsly, J. Phys. Chem. 100 (1996) 5745.
[22] M.H. Hennessy, Y. Wu, A.B. Bocarsly, Z.G. Soos, J. Phys. Chem. A 102 (1998) 8312.
[23] S.K. Doorn, J.T. Hupp, J. Am. Chem. Soc. 111 (1989) 1142.
[24] G.C. Walker, P.F. Barbara, S.K. Doorn, Y. Dong, J.T. Hupp, J. Phys. Chem. 95 (1991) 5712.
[25] B.W. Pfennig, J.V. Lockard, J.L. Cohen, D.F. Watson, D.M. Ho, A.B. Bocarsly, Inorg. Chem. 38 (1999) 2941.
[26] F. Scandola, C.A. Argazzi, C. Bignozzi, C. Chiorboli, M.T. Indelli, M.A. Rampi, Coord. Chem. Rev. 125 (1993) 283.
[27] K. Nakamoto, Infrared and Raman Spectra of Inorganic and Coordination Compounds, fourth ed., Wiley, New York, 1986.
[28] D.R. Lombardi, C. Wang, B. Sun, A.W. Fountain, III, T.J. Vickers, C.K. Mann, F.R. Reich, J.G. Douglas, B.A. Crawford, F.L. Kohlasch, Appl. Spectrosc. 48 (1994) 875.
[29] G.A. Neyart, J.T. Hupp, J.C. Curtis, C.J. Timpson, T.J. Meyer, J. Am. Chem. Soc. 118 (1996) 3724.
[30] R.A. Marcus, Rev. Mod. Phys. 65 (1993) 599.
[31] V. Gutmann, The Donor–Acceptor Approach to Molecular Interactions, Plenum Press, New York, 1978.
[32] D.A.V. Kliner, K. Tominaga, G.C. Walker, P.F. Barbara, J. Am. Chem. Soc. 114 (1992) 8323.
[33] K. Tominaga, D.A.V. Kliner, A.E. Johnson, N.E. Levinger, P.F. Barbara, J. Chem. Phys. 98 (1993) 1228.
[34] R.A. Marcus, J. Phys. Chem. 93 (1989) 3078.